Published in final edited form as:
Dev Biol. 2012 March 1; 363(1): 84–94. doi:10.1016/j.ydbio.2011.12.023.

The cytokine macrophage migration inhibitory factor (MIF) acts as a neurotrophin in the developing inner ear of the zebrafish, *Danio rerio*

Yu-chi Shen[a], **Deborah L. Thompson**[a,e,1], **Meng-Kiat Kuah**[b,c], **Kah-Loon Wong**[b], **Karen L. Wu**[a], **Stephanie A. Linn**[a], **Ethan M. Jewett**[d], **Alexander Chong Shu-Chien**[b,c], and **Kate F. Barald**[a,e]

[a]Department of Cell and Developmental Biology, Medical School, University of Michigan, Ann Arbor, Michigan, USA

[b]School of Biological Sciences, Universiti Sains Malaysia 11800, Minden, Penang, Malaysia

[c]Malaysian Institute of Pharmaceuticals and Nutraceuticals, Malaysian Ministry of Science, Technology and Innovation, 62662 Putrajaya, Kuala Lumpur, Malaysia.

[d]Bioinformatics Program, University of Michigan, Ann Arbor, MI

[e]Department of Biomedical Engineering, College of Engineering, University of Michigan, Ann Arbor, MI

Abstract

Macrophage migration inhibitory factor (MIF) plays versatile roles in the immune system. MIF is also widely expressed during embryonic development, particularly in the nervous system, although its roles in neural development are only beginning to be understood. Evidence from frogs, mice and zebrafish suggests that MIF has a major role as a neurotrophin in the early development of sensory systems, including the auditory system. Here we show that the zebrafish mif pathway is required for both sensory hair cell (HC) and sensory neuronal cell survival in the ear, for HC differentiation, semicircular canal formation, statoacoustic ganglion (SAG) development, and lateral line HC differentiation. This is consistent with our findings that MIF is expressed in the developing mammalian and avian auditory systems and promotes mouse and chick SAG neurite outgrowth and neuronal survival, demonstrating key instructional roles for MIF in vertebrate otic development.

Keywords

Zebrafish; macrophage migration inhibitory factor; inner ear; sensory HC; statoacoustic ganglion; immune cytokines; neurotrophin

Corresponding Author: Kate F. Barald Ph.D. kfbarald@umich.edu Department of Cell and Developmental Biology 3053 BSRB 2200 109 Zina Pitcher Place Ann Arbor, MI, 48109-2200 USA Telephone: 734-647-3376 Fax: 734-763-1166.
[1]Present address: Department of Internal Medicine, Division of Pulmonary and Critical Care Medicine, University of Michigan

Introduction

Critical extracellular signals are involved in the development of vertebrate inner ear innervation (Barald and Kelley, 2004). Cultured mouse and chick otocysts release protein(s) collectively termed otocyst-derived factor (ODF) that promote neurite outgrowth and survival of embryonic statoacoustic ganglion (SAG) neurons *in vitro*, which are also thought to direct innervation *in vivo* (Ard, et al., 1985; Lefebvre et al., 1990; Bianchi & Cohan, 1991; Bianchi et al., 2005). These functions have been thought to be controlled by neurotrophins (neurotrophic factors), defined as target-generated directional neurite outgrowth promoting and neuronal survival promoting factors such as nerve growth factor (NGF; Purves et al., 2001). However, proteomic and array analysis of ODF demonstrates that it does not contain any known classical neurotrophins (Bianchi et al., 2005), suggesting that ODF growth factor(s) that promote the initial outgrowth and survival of SAG neurons are novel. Faced with the apparent paradox of neurotrophic action in the absence of classical neurotrophic factors, we set out a number of years ago to determine which components in ODF fulfilled that role *in vivo* and *in vitro*.

Both our earlier (Bianchi et al., 2005) and recent work (Bank et al., submitted) demonstrate/d that chick and mouse otocyst-derived ODF includes at least 3 “immune system” cytokines, one of which is the immune system “inflammatory” cytokine macrophage migration inhibitory factor (MIF; Bank et al., submitted). MIF, known for its involvement in T-cell (Larson and Horak 2006) and B-cell development (Takahashi et al., 1999); shares no sequence similarity with classical neurotrophins or with other known cytokines (Weiser et al., 1989), but is related to D-dopachrome tautomerase (DDT) (Esumi et al., 1998). We found both MIF (mif) and the tautomerase (mif-like) expression in the zebrafish. In mammals, MIF protein and mRNA are expressed in CNS neurons (Nishino et al., 1995; Bacher et al., 1997; Bacher et al., 1998) and MIF is involved in neuronal degeneration-regeneration processes (Yoshimoto et al., 1997; Nishio et al., 1999; Koda et al., 2004). Most significantly, MIF mRNA is found in the developing neuraxes and nervous systems of *Xenopus* (Suzuki et al., 2004), mouse (Kobayashi et al., 1999) and zebrafish (Ito et al., 2008, Holmes et al., 2011) and is a critical player in establishing the neuraxis of the embryo (Suzuki et al., 2004).

MIF is found in the developing inner ear of both *Xenopus* (Suzuki et al., 2004), and zebrafish (Ito et al., 2008, Holmes et al., 2011). MIF message and protein are also found in the mouse (Kobayashi et al., 1999) and chick (Bank et al., submitted) inner ears in early pre-sensory regions of the otocyst and in supporting cells in adults. $MIF^{-/-}$ mice are hearing-impaired as early as 4 weeks postnatally, with significantly fewer spiral ganglion neurons (SGN) and sensory HC than wild-type mice of the same genetic background (Bank et al., submitted).

The best-known MIF receptor, CD74 (Leng et al., 2003), is expressed on the surface of inner ear neurons. In the mouse and chick, we have found that CD74 is found on both early stage SAG and adult SGN (Bank et al., submitted). Two zebrafish homologues of CD74, invariant chain like protein 1 and 2, (iclp1, 2, recently renamed cd74a and cd74b respectively), have been cloned (Yoder et al., 1999), but their embryonic expression patterns had not previously been described prior to this report.

In this study, we have explored the MIF signaling components and further defined their function by knockdown with antisense oligonucleotide morpholinos (MOs) or, in parallel experiments, with a biochemical MIF inhibitor. We report the developmental expression of the second zebrafish mif family member, mif-like, and the expression patterns for the

receptors for both mif and mif-like receptors, iclp1 and iclp2 in the embryo and in the inner ear.

We found that perturbations of MIF signaling resulted in a significant reduction in the size of the SAG, the number of sensory HC and the size of the brain in zebrafish. We demonstrate that these reductions take place, at least in part, by a p53-dependent mechanism. Both MIF-dependent mouse macrophage survival (Mitchell et al., 2002) and MIF's ability to prevent apoptosis in regenerating rat peripheral nerve Schwann cells (Nishio et al., 2002) also depend on MIF inhibition of p53-dependent apoptosis. Therefore, the involvement of p53—at least in part-- in MIF regulation of both sensory hair cell numbers and numbers of SAG neurons is consistent with the involvement of MIF and p53 in apoptosis in other systems.

Material and Methods

Zebrafish Maintenance, embryos collection, and embryo husbandry

Wild type zebrafish were obtained from University Aquarium, Ann Arbor or local pet stores, Penang, Malaysia and kept on a 14:10 hr light/dark cycle at 28.5°C. Embryos were raised at 28.5°C in methylene blue (0.3 ppm) fish water to prevent fungal growth. For in situ hybridization (ISH) experiments, 0.03% 1-phenyl-2-thiourea ($C_6H_5NaHCSNH_2$/PTU, Sigma) was added (1:10) around 12 hpf to prevent pigmentation. Embryos were observed or fixed in 4% paraformaldehyde (PFA) in phosphate buffered saline (PBS; 1×PBS, pH 7.3) at the time/stage indicated, rinsed with PBST (0.1% Tween-20 in 1xPBS), and dehydrated in Methanol and stored at -20°C. These methods were adapted from Westerfield (2000). The mif inhibitor, 4-iodo-6-phenylpyrimidine (4-IPP; Specs, Delft, Netherlands), was used to treat embryos at 6-7 hpf immediately after dechorionation with 10 mg/ml Pronase (2 min, and 2x rinse with fish water). The embryos were incubated in 30-40 μM 4-IPP in 32 mM DMSO, at 28.5°C until observation or fixation for further reactions and subsequent observation.

RT-PCR Analysis

To assay developmental expression of *mif* and *iclp* transcripts, total whole embryo RNA was isolated with Trizol (Invitrogen). RNA was reverse-transcribed with the Superscript III system (Invitrogen) and PCR performed using Jumpstart Taq polymerase (Sigma-Aldrich).

The fragments amplified are nucleotides 15-526 for *mif-like*, 98-620 for *iclp1*, and 51-575 for *iclp2*. Primer positions used in these studies are illustrated in Fig. 1. The predicted size of the RT-PCR products is 512 bp for *mif-like* primer pair, 523 bp for *iclp1*, and 525 bp for *iclp2*, respectively.

In Situ Hybridization

RT-PCR was used to amplify cDNA fragments for probe templates and RT-PCR products cloned into the pCRII-TOPO vector (InVitrogen) and digested with either EcoRV or BamHI restriction enzymes to produce templates for sense and antisense probes, respectively. After column purification of digested template DNA (MinElute Reaction Cleanup kit, Qiagen), synthesis was performed using a DIG RNA label with T7 polymerase or SP6 polymerase. Whole mount ISH was performed as previously described (Shen et al., 2008). Hybridizations were detected using an alkaline-phosphatase-conjugated antibody and visualized with 4-nitroblue tetrazolium/5-bromo-4-chloro-3-indolyl phosphate (NBT/BCIP; Roche). Embryos were observed under a Leica MXFL III stereo dissecting microscope; photos were taken with an Olympus DP-71 Digital camera and processed with Adobe@

Photoshop. Sections were observed and photographed with an Olympus BX-51 compound microscope.

Morpholino Injections

Morpholinos (MOs, Gene Tools, Corvallis, OR) were designed based on zebrafish genomic sequences of *mif, mif-like, iclp1, and iclp2*: An antisense MO, complementary to the start codon of zebrafish *mif* mRNA: 5'-ACATCGGCATGACTGCGACAGAGAT-3'. Two MOs were used for *mif-like*. *mif-like* MO1is complementary to the translational start site: 5'-GTTTCTATATTTATGAACGGCATGA-3', while *mif-like* MO2 derived from AS sequence at the intron1/exon 2 boundary: 5'-GATTCATCCTCTGAAGACGTAAGCC-3'. MOs are complementary to the boundary of exon2 and intron 2 of *iclp1* and *iclp2* pre-mRNA: *iclp1*MO: 5'-TGTTTTGTGTGTTTACGCACCTGAC-3'; *iclp2*MO: 5'-CGTGCTATGGTTTTCTGACCAGATT-3'. Control MO was the scrambled nucleotide sequence from Gene Tools: 5'-CCTCTTACCTCAGTTACAATTTATA-3'.

MOs were microinjected into the yolk of 1-8 cell embryos with a PV820 Pneumatic PicoPump (World Precision Instruments) and an attached Nitrogen tank according to our previously published procedures (Shen et al., 2008). Injection conditions: volumes of either 1nl or 2nl: 0.3 mM for *mif, mif-like* MO1, and *mif-like* MO2. *iclp* MOs were used in combination (0.5 mM for *iclp1* MO,1 mM for *iclp2* MO). Five nanograms of p53 MO was combined in the 0.3 mM *mif* MOs. RNA prepared from injected embryos at 50 hpf was reverse-transcribed and amplified with primer sets for *mif-like, iclp1*, and *iclp2* to evaluate the efficacy of knockdown with *mif-like* MO2, *iclp1*, and *iclp2*, respectively. RT-PCR products were separated by size on 1.5% agarose gels, visualized by ethidium bromide.

Morphology and Cell death assays

Injected fish were observed between 25 hpf and 48 hpf under a MXFL III microscope (Leica). Acridine Orange [AO, 3, 6-bis(dimethylamino) acridine zinc chloride double salt; Sigma] was used to detect cell death in embryos as described previously (Shen et al., 2004). Living embryos were dechorionated and stained with 5 μg/ml AO in embryo-rearing media (Westerfield, 2000) for 10 min and then rinsed with media. Dead cells incorporating AO were visualized with a MXFL III stereo microscope with a fluorescent channel (Absorption 460-550 nm, Beam splitter 505 nm, and Emission at 510 nm), and photographed with an Olympus DP-71 Digital camera. AO-labeled cells were counted with the magnified photograph using Adobe@ Photoshop.

Actin and zn-5 Staining

Embryos or larvae were fixed in 4% PFA/PBS, treated with PBS/1.5% Triton X-100 for 1- 2 days at 4°C, incubated with Texas red-phalloidin (1:200 dilution, Molecular Probes) in PBS/BSA/DMSO (PBD; Westerfield, 2000) overnight at 4°C and rinsed multiple times with PBD. For zn-5 immunolabelling, embryos were incubated with zn-5 antibody (1:500 dilution, ZIRC) followed by Alexa Fluor 488-goat anti-mouse secondary antibody (Molecular Probes). Embryos or larvae were viewed with an Olympus FV500 confocal microscope. The z-stack of confocal pictures as well as the SAG were outlined and the area of the SAG calculated with MetaMorph@ image analysis software.

Lateral Line (LL) Hair Cell Staining

Physiologically active HC in neuromasts were labeled by exposure to 4-Di-2-ASP (4-(4-Diethylaminostyryl)-1-methylpyridinium iodide, Sigma D-3418) (previously described: Shen et al., 2008). Embryos or larvae were incubated in 0.005% 4-Di-2-ASP in fresh

embryo water (Westerfield, 2000) 28.5°C /30 min. After a short embryo water rinse, embryos or larvae were observed and photographed under a MXFL III microscope.

RNA-mediated Gain of Function (rescue) Experiments

Open reading frames (ORFs) of *mif, mif-like, iclp1* and *iclp2* were amplified using RT-PCR and cloned into pCS2+ vector. Capped RNA was synthesized using a mMESSAGE mMACHINE Sp6 in vitro transcription kit (Ambion Inc., Austin, TX). RNAs were diluted into 100ng/μl and co-injected with the corresponding morpholinos.

Statistical treatment of data—One-tailed T-tests were used to assess the significance of the data. The error bars indicate standard deviation.

Results

Expression patterns of zebrafish *mif* and *mif-like*

Two zebrafish *mif-like* genes, one with higher homology to the mammalian *MIF* gene, and the other with a higher homology to the mammalian *DDT* gene were identified in a GenBank search. The first cDNA delineating complete *mif* cDNA (GenBank ID: DQ639953.1), matched the DNA sequence from clone DKEYP-121D2 on chromosome 14 (NCBI Reference Sequence ID: NC_007125.4; Ito et al., 2008). The second cDNA, which we named *mif-like*, (GenBank ID: BC071391.1), was mapped to sequences from *Danio rerio* chromosome 21 (NCBI Reference Sequence ID: NC_007132), syntenic to the human *MIF* and *DDT* genes on chromosome 22q11.23 (http://uswest.ensembl.org). The zebrafish *mif* coding sequence predicts a protein with 115 amino acids, the same as mammalian MIF (Weiser et al., 1989). The predicted protein is 69% identical to human MIF. The gene structure of the zebrafish *mif* is very similar to that of human *MIF*, with only slight variations in exon length and large variations in intron length (Fig. 1A).

The coding region of the zebrafish *mif-like gene* encodes a predicted protein of 118 amino acids, the same size as the mammalian DDT (Esumi et al., 1998). Mif-like protein is less homologous to the mammalian proteins. Both zebrafish mif and mif-like contain all of the amino acid residues conserved among all *MIF* family genes found in different species (Esumi et al., 1998). The gene structure of *mif-like* is the same as the human DDT, although the non-coding exon1 in human DDT has not been found in the *mif-like* gene (Fig. 1A).

Developing zebrafish mRNA expression patterns for *mif* and *mif-like* are very similar, with stronger expression of the *mif* signal. We detected *mif* signal as early as 12 hpf in the anterior part of the embryos (Figs. 2B, F), and as shown in Ito et al., (2008), *mif* mRNA is expressed strongly in the midbrain and eye at 24 hpf (Fig. 2J), and in the midbrain at 36 hpf and 48 hpf (Figs. 2N, O), when eye expression is reduced. Branchial arches and pectoral pin buds also express *mif*. Expression of *mif* is detected in the otic vesicle (Figs. 2J, N, O, and R), which was not mentioned in Ito et al., (2008). Sections through the otocyst showed that *mif* is expressed in the lateral epithelial cells (Fig. 2O inset).

Mif-like mRNA is detected by 12 hpf by RT-PCR; levels become higher at 26 hpf and remain throughout the stages tested till 72 hpf (Fig. 2A). Whole mount ISH shows that *mif-like* is expressed in the eye, strongly in the lens, moderately in the otic vesicle and weakly in the brain at 24 and 36 hpf (Figs. 2L and P). The expression in the lens is reduced by 48 hpf (Fig. 2Q), but moderate expression in the otic vesicle and brain is detectable until at least 72 hpf (Figs. 2Q, T). In the otic vesicle, *mif-like* is detected in the lateral epithelial cells and very weakly in the hair cells of the anterior macula (Fig. 2Q inset). No expression was detected with any of the sense probes (Figs. 2C, E, G, I, K, M, S and U). This expression

pattern is very similar to that of stage 34 *Xenopus Mif* (Suzuki et al., 2004) and embryonic mouse *Mif* expression (Kobayashi et al., 1999) in the brain, eye capsule and otocyst. Expression of zebrafish *mif* and *mif-like* has not been detected in fish somites as in mouse (Kobayashi et al., 1999) and *Xenopus*. Zebrafish *mif* and *mif-like* are expressed prominently in the inner ear at times of critical differentiation steps in its development, including SAG delamination and formation, implying their roles in the process.

Expression patterns of zebrafish *iclp1* and *iclp2*

Two zebrafish homologs of the mammalian MIF receptor, CD74, have been cloned and named invariant chain-like proteins 1 and 2 (Iclp1 and Iclp2, GenBank ID: AF148214 and AF116539, respectively; Yoder et al., 1999). Based on the overall homology and predicted structures, iclp1 is more likely to be functionally equivalent to mammalian CD74 (Yoder et al., 1999). Abundant expression of both *iclp1* and *-2* is detected in the adult kidney, and much lower levels of expression are found in the spleen, liver, and intestine (Yoder et al., 1999). We examined the expression of *iclp1* and *iclp2* in embryonic zebrafish. Both genes are expressed as early as 12 hpf, with *iclp1* weaker at this stage, and throughout the stages tested (72 hpf). Although expression levels of both genes fall at 36 hpf, higher levels are again seen at 72 hpf (Fig. 3A). Whole mount ISH experiments showed weak expression of *iclp1* at 14 hpf in the anterior part of the embryo (Fig. 3B), and in the otic vesicle at 24 hpf, 36 hpf, 48 hpf and 72 hpf (Figs. 3D, F, G and H); *iclp2* was expressed at a moderate level at 14 hpf (Fig. 3K), weakly in the otic vesicle at 24 hpf (Fig. 3M), and at higher levels at 36, 48, and 72 hpf (Figs. 3O, P, and Q). In sectioned developing otocysts, we found that both *iclp1* and *iclp2* were expressed in the lateral epithelial cells of the otocyst (Fig. 3G and P insets). Additionally, iclp1 is expressed in the hair cells (HC) of both the anterior macula (Figs. 3I and J) and posterior macula (Fig. 3G inset). Very weak expression was also detected in the SAG at the same stage (Fig. 3I). There is also expression of *iclp1* at 36 and 48 hpf in the pectoral fin bud (Figs. 3F and G). No signal was detected with sense probes (Figs. 3C, E, L, N, and R). That zebrafish mammalian CD74 homologs are present in the developing inner ear further supports a role for *mif* in inner ear development.

From 24 hpf on, *iclp1* is expressed in lateral line (LL) neuromasts (Figs. 3D, F, G, and H), more strongly in the anterior than posterior LL, indicating it might also be involved in LL development.

Mif pathway is important for the morphogenesis of zebrafish embryos

The expression of *mif*, *mif-like*, *iclp1*, and *iclp2* in the otic vesicle during inner ear morphogenesis, especially SAG delamination and HC differentiation, suggested that the mif pathway might be involved in these processes. We therefore combined *mif* and *mif-like* MOs for injections to produce *mif* morphants, and *iclp1* and *iclp2* MOs to obtain *iclp* morphants.

To examine the efficacy of the MOs, we isolated total RNA from controls, morphants, and morphants that had also received capped RNA injections at 50 hpf, performing RT-PCR to amplify regions containing the predicted splice-blocking sites (Figs. 1A, B). *Mif-like* MO2 blocks the splicing of intron 1, resulting in the deletion of exon 2. The predicted mRNA is 176 bp shorter than the normal transcript. As shown in Fig. 4A, *mif* morphants had both a shorter transcript and a much reduced quantity of the normal one. With coinjection of *mif-like* capped RNAs, the amount of normal transcript increased, although not to the level of the control, and a reduced amount of the shorter fragment without exon2 was also detected. This could have led to low efficiency of rescue (see below). For both *iclp1* and *iclp2*, shorter fragments were not detected in morphants (Fig. 4B), but the levels of the normal mRNAs were largely decreased compared to those of the controls (Fig. 4B). This could be due to the

instability of the shorter mRNA, as we also observed in Shen et al., (2008). With RNA "rescue", levels of the normal transcript were regained (Fig. 4B).

Iclp1 and *iclp2* morpholinos alone caused many fewer phenotypic changes than *mif* MOs, even at 1 mM and 2 mM, respectively (data not shown). However, the combination of *iclp1* and *iclp2* morpholinos at 0.5 mM and 1mM resulted in ventrally curled embryos, while the size of the brain was not greatly reduced (Figs. 5C and R). This is contrary to what is seen with the *mif* morphants, which have much smaller heads and overall attenuated nervous systems, including the eye and the ear regions (Figs. 5B and Q).

Several chemicals inhibit MIF, including (S,R)-3-(4-hydroxyphenyl)-4, 5-dihydro-5-sioxazole acetic acid methyl ester (ISO-1; Lubetsky et al., 2002), a fluorinated analog of ISO-1, ISO-F (Dagia et al., 2009), Trichostatin A (TSA; Lugrin et al., 2009), and 4-iodo-6-phenylpyrimidine (4-IPP; Winner et al., 2008). All of these chemicals but TSA inhibit mif dopachrome tautomerase activity in vitro (Lubetsky et al., 2002; Winner et al., 2008; Dagia et al., 2009). TSA is a histone deacetylase inhibitor that inhibits mif transcription through a local chromatin deacetylation (Lugrin et al., 2009), but it also affects expression of other genes as well as inducing cell cycle arrest and cell death (Noh et al., 2009).

We have examined the impact of ISO-1 and 4-IPP on zebrafish embryonic development, and found 4-IPP to be much more potent than ISO-1 (data not shown); hence we used 4-IPP for all further experiments. The effect of 4-IPP on embryos is dose-dependent. With more than 50 μM 4-IPP, more than half of the embryos did not survive for 2 days. Therefore, the highest concentration used for 4-IPP incubation was 40 μM. We found that treatment with 4-IPP resulted in less pigmentation and in minor gross defects in the embryos (Fig. 5E) when compared to the DMSO control (Fig. 5D), but the chemical inhibitor's effect is much less pronounced than the effects of *mif* or even *iclp* morpholino injections. However, when we examined these embryos at later stages, we found remarkable ear defects in these embryos (see below).

As Ito et al., (2008) had previously observed, we saw dramatically increased cell death in the brain of *mif* morphants (Fig 5G) compared to control MO-injected embryos (Fig. 5F). The AO-positive cells are spread throughout the otocyst in *mif* morphants (Fig. 5U). However, consistent with the results on embryo size, cell death in the brain of *iclp* morphants was not as pronounced as in *mif* morphants (Figs. 5H, M). Quantitative results showed that the number of dead cells found in the ear doubled in *mif* morphants. This increased cell death could be partially rescued by *mif* RNA injection (Fig. 5S) or by injection of 5 ng of *p53* MO (Fig. 5T). There was a slight increase in cell death in 4-IPP-treated embryos as well (Figs. J and O) compared to embryos treated with DMSO vehicle only (Figs. 5I and N).

Mif pathway and zebrafish inner ear development

Ito et al. (2008) demonstrated that *mif* is critical for brain and optic vesicle development. The effects of *mif* MOs in the otic vesicle were not examined in that report. To investigate the role of the mif pathway in inner ear development, we first performed whole mount ISH with several inner ear markers, including *fgf8*, *dlx3b*, *dlx4b*, *tlxA*, and *pax2b*. Expression patterns of these genes were not different between the *mif* morphants and controls (data not shown), indicating that early events of inner ear development such as organogenesis and specification were not affected by the *mif* MOs. However, increased cell death in the inner ear could result in defects of inner ear structure. To detect any fine structural changes in *mif* morphants, we used confocal microscopy to observe sensory HC patches, formation of semicircular canals, and SAG development.

The three cristae in the *mif* and *iclp* morphants were normal in shape and kinocilia length (data not shown). However, when the stereocilia were stained with phalloidin, reduced HC numbers were observed in the saccular macula in both *mif* (Figs. 6B and G) and *iclp* morphants (Figs. 6D and I) at 3dpf and 6 dpf, although the numbers of HC continued to increase over time (Fig. 6K). A similar reduction in phalloidin-positive cells in the morphants was detected in the utricular macula (data not shown). Concomitant RNA injection partly rescued macular HC development (Figs. 6C, E, H, J, and K).

4-IPP also reduced the number of hair cells stained with phalloidin at 4 dpf in a dosage-dependent manner (Fig. 6L), further supporting the importance of mif function in HC development.

Formation of semicircular canals (SCC) was also defective in the *mif* morphants. By 3 dpf, epithelial pillars should have formed from the fusion of the central bulges and the peripheral projections from all directions (anterior, posterior, and ventral; Figs. 7A, F, and K; Waterman and Bell, 1984). However, in more than half of the *mif* morphants, fusion of the bulges and the projections was incomplete (Fig. 7B). This is not likely due to developmental delay, because fusion failure was found in morphants at much later stages (4 and 5 dpf, Figs. 7G, and L, respectively). The defects were seen in all three canals, but the posterior and ventral SCC were more affected. In morphants co-injected with capped RNA, normal SCC formation was largely restored (Figs. 7C, H, and M). The defects of SCCs in the *iclp* morphants (Figs. 7D, I, and N) were much milder than in mif morphants. RNA injections almost always completely rescued the canal phenotype of the *iclp* morphants (Figs. 7E, J, and O). Embryos and larvae treated with 4-IPP had similar defects in SCC formation, although these were not as severe as *mif* morphants (data not shown).

Mif signalling and cranial ganglia development

Recombinant Mif promotes isolated SAG neurite outgrowth and survival in chick and mouse (Bank et al., submitted). To determine whether mif has the same function in zebrafish, we examined morphant SAGs as well as SAGs from 4-IPP-treated embryos. To observe early stage SAG development, we performed whole mount ISH using an *nkx5.1* (*hmx3*) probe. The expression of *nkx5.1/hmx3* is detected in the otic placode and vesicle and in the cells forming the SAG (Adamska et al., 2000; Feng and Xu, 2010). Our results showed reduced signal of *nkx5.1* in the developing ear and SAG in *mif* morphants (Fig. 8B), *iclp1* morphants (Fig. 8D), and mif inhibitor (4-IPP) treated (40 μM) embryos (Fig. 8F), indicating a reduction in SAG neuroblasts. 4-IPP at 30 μM did not cause as much reduction of *nkx5.1* expression (Fig. 8E) as 40 μM. Monoclonal antibody zn-5 was used to label differentiating neurons and their processes at 48 hpf. Zn-5 can be used to label the SAG, trigeminal cranial ganglia, and anterodorsal lateral line ganglia (gAD) (Wilson et al., 2007). *Mif* MOs treatment resulted in much smaller SAGs and gADs (Fig. 8H) compared to controls (Fig. 8G), while *iclp* MOs did not have a significant effect on the size of the ganglia (Fig. 8J). Neuronal processes in the brain are also shorter in *mif* morphants (Fig. 8H). Concomitant RNA injection improved both the sizes of the ganglia (Figs. 8I, K, and L) and length of the neuronal processes (data not shown).

Iclp and lateral line (LL) development

iclp1 expression in lateral line (LL) neuromasts suggests that it has a function in LL development. We investigated active neuromast HC with a mitochondrial dye, 4-Di-2-ASP. 4-Di-2-ASP staining of *iclp* morphants showed that LL promordia have reached the tail by 72 hpf (Fig. 9B), but there were fewer active neuromasts in both anterior and posterior LLs (Fig. 9H). Phalloidin staining of neuromast HC also showed reduced postive cell numbers in *iclp* morphants (Fig. 9E) compared to controls (Fig. 9D), indicating that there are HC defects

in the neuromasts of the LL. In additional experiments in which capped RNA for both receptors was introduced along with the MOs, a partial rescue was achieved (Figs. 9C, FG and data not shown).

Discussion

That immune system cytokines play important neurotrophic roles in the developing nervous system is not a new idea (reviewed in Deverman and Patterson, 2009), but the identification of MIF (mif)'s neurotrophic roles in the early developing inner ear and its effects on both innervation and sensory hair cell development is novel. Zebrafish in which mif was knocked down with MOs have a reduced neuronal complement of the SAG (Fig. 8), which can be rescued by co-injection of capped mif RNA.

Based on the work of Suzuki et al. (2004) in *Xenopus*, effects on neurulation and neural axis formation were expected in our experiments; injections of MOs to both *mif* and *mif-like* in combination, reduced the overall size of the CNS through apoptosis. However, because such effects could represent non-specific toxic effects of MOs introduced into the 1-8 cell stage embryo, which has effects on the brain and other parts of the CNS as well as the ear, we have also successfully introduced combined MOs directly into the nascent zebrafish inner ear at 24 hpf and electroporated them into specific ear quadrants (Holmes et al., 2011). We found that we can specifically alter inner ear development and innervation without affecting nervous system development in the embryos in which the otic vesicle alone was injected (Holmes et al., 2011). The possible toxic effects of MOs on whole embryos injected at the 1-8 cell stages are therefore not affecting inner ear differentiation.

We only observed partial rescue with RNA injections in *mif* morphants, in which the levels of the normal *mif-like* transcript were drastically lowered and a transcript with exon2 spliced out was detected. When capped RNAs were co-injected, the shorter transcript without exon2 was observed and it is possible that this results in a dominant negative protein. Our results from 4-IPP treatment showed that blocking mif-function at the protein level had similar effects on inner ear development, further strengthening the idea that mif is a significant player in inner ear organogenesis.

Consistent with our studies of MIF function in SAG development in both mouse and chick (Bank et al., submitted), the results of these studies showed that the *mif* pathway also plays crucial roles in zebrafish inner ear development. Our results also agreed with those of Ito et al. (2008) in that, although *mif* MOtreatment did not completely abolish zebrafish axis formation as was found in *Xenopus* (Suzuki et al., 2004), the nervous system has been severely compromised, including the brain, the eye, and the ear.

We have shown that *mif*, *mif-like*, *iclp1*, and *iclp2* genes are expressed in the ear, in addition to the brain and the eye, and the timing of their expression coincides with critical stages in inner ear development. The *mif* morphants had smaller brains, and increased cell death in both the brain (as also observed by Ito et al., 2008) and in the ear as shown in this report. However, the gross morphology of the morphant ears was not affected, and early ear markers were present in the same patterns as in normal control embryos, suggesting that although the *mif* pathway has a role in early neurogenesis, it does not affect the early gross morphogenesis of the inner ear. Instead, it has a recurrent role at later stages including specification, differentiation, and maturation of individual inner ear cell types.

The increased cell death seen in *mif* morphants is consistent with the role of mammalian MIF in preventing apoptosis in cells of the immune system (Nishio et al., 2002). In the mammalian system, MIF is thought to block apoptosis by inhibiting p53 activity (Mitchell et al., 2002). Our results showed that a high concentration of *p53* MO can rescue the cell death

caused by *mif* MOs, indicating an involvement of p53 activity in the pathway. Understanding the detailed pathway by which mif inhibits cell death in the zebrafish ear awaits further investigation.

In addition to increased cell death, *mif* morphants had deformed SCC, reduced HC/stereocilia, and much smaller SAGs. *Iclp* morphants had fewer HC stained with phalloidin, as did the *mif* morphants, but their semicircular canals and SAGs were not significantly impacted. It is possible that there is one or more receptor other than the mammalian CD74 orthologs for mif in the zebrafish, and that the functions are split among the receptors. As mentioned earlier, CD44 is found to be expressed on pillar cells in the inner ear in the Tunnel of Corti (Hertzano et al., 2010).

It is possible that there are additional MIF receptors in addition to CD74, in the inner ear. Mif acts as a ligand of CXC chemokine receptors to stimulate immune cells (Bernhagen et al., 2007), including Cxcr2 and Cxcr4. However no expression of cxcr2 in the developing inner ear has yet been reported and we found none.

Cxcr4 is widely expressed in the vertebrate CNS (Zou et al., 1998; McGrath et al., 1999; Tissir et al., 2004; Tiveron & Cremer, 2008). Two zebrafish *cxcr4* orthologs have been found. In addition to early expression of *cxcr4* genes in lateral mesoderm and posterior midbrain, interneurons and endoderm, sensory neurons, motorneurons and cerebellum as well as the eye (Chong et al., 2001), *cxcr4b* is expressed in the leading cells of the migrating LL primordia (Dambly-Chaudière et al., 2007; Valentin et al., 2007). It is required for the migration of the posterior LL primordia (Dambly-Chaudière et al., 2007; Valentin et al., 2007). The expression of *cxcr4* in the developing zebrafish ear has not been studied in detail, but preliminary ISH results indicated that there is expression of *cxcr4b* in the region of the ear (Dambly-Chaudière et al., 2007). However inner ear or later LL system expression remains to be investigated. It will be intriguing to examine the roles of both cxcr2 and cxcr4 in lateral line development, and to determine whether they function as mif receptors in this tissue.

Since ODF is composed of numerous bioactive factors, most of which are cytokines and many of which play neurotrophic roles in other parts of the nervous system (Bianchi et al, 2005), we need to investigate them sequentially to understand the interaction(s) between/among them. It is likely that there is crosstalk among members of different cytokine subfamilies and the receptors that signal to promote SAG neurite outgrowth. Dissecting the ODF cytokine-based “network” will help us understand the mechanism of how cytokines function in inner ear development and, potentially, in SAG regeneration, since the mature form of the SAG in mammals, the spiral ganglion retains receptors for MIF (Bank et al., submitted).

Acknowledgments

Confocal images were acquired at the UM Diabetes Center Microscopy facility (NIH P60-DK20572). Support is gratefully acknowledged from the following sources: KFB: NIH/NINDCD 2 RO1 DC04184, 3R01DC004184-08W1, NSF DBI 0832862, NSF IOS 0930096. Y-cS: Deafness Research Foundation (DRF). DLT: DRF. ACS-C: Fulbright Fellowship (USA/Malaysia) supported sabbatical at U Michigan and MOSTI ESCIENCE grant 305/PBIOLOGI/613220. SAL: TEAM NIH T32 fellowship at Michigan. KMK: MOSTI NSF Scholarship; EMJ: Genome Sciences (NIH) Training Grant T32 HG00040, University of Michigan.

References

Adamska M, Leger S, Brand M, Hadrys T, Braun T, Bober E. Inner ear and lateral line expression of a zebrafish Nkx5-1 gene and its downregulation in the ears of FGF8 mutant, ace. Mech. Dev. 2000; 97:161–165. [PubMed: 11025218]

Ard MD, Morest DK, Hauger SH. Trophic interactions between the cochleovestibular ganglion of the chick embryo and its synaptic targets in culture. Neuroscience. 1985; 16:151–170. [PubMed: 3835500]

Bacher M, Meinhardt A, Lan HY, Dhabhar FS, Mu W, Metz CN, Chesney JA, Gemsa D, Donnelly T, Atkins RC, Bucala R. MIF expression in the rat brain: implications for neuronal function. Mol. Med. 1998; 4:217–230. [PubMed: 9606175]

Bacher M, Meinhardt A, Lan HY, Mu W, Metz CN, Chesney JA, Calandra T, Gemsa D, Donnelly T, Atkins RC, Bucala R. Migration inhibitory factor expression in experimentally induced endotoxemia. Am. J. Pathol. 1997; 150:235–246. [PubMed: 9006339]

Barald KF, Kelley MW. From placode to polarization: new tunes in inner ear development. Development. 2004; 131:4119–4130. [PubMed: 15319325]

Bernhagen J, Krohn R, Lue H, Gregory JL, Zernecke A, Koenen RR, Dewor M, Georgiev I, Schober A, Leng L, Kooistra T, Fingerle-Rowson G, Ghezzi P, Kleemann R, McColl SR, Bucala R, Hickey MJ, Weber C. MIF is a noncognate ligand of CXC chemokine receptors in inflammatory and atherogenic cell recruitment. Nat. Med. 2007; 13:587–596. [PubMed: 17435771]

Bianchi LM, Cohan CS. Developmental regulation of a neurite-promoting factor influencing statoacoustic neurons. Brain Res. Dev. Brain Res. 1991; 64:167–174.

Bianchi LM, Daruwalla Z, Roth TM, Attia NP, Lukacs NW, Richards AL, White IO, Allen SJ, Barald KF. Immortalized mouse inner ear cell lines demonstrate a role for chemokines in promoting the growth of developing statoacoustic ganglion neurons. J. Assoc. Res. Otolaryngol. 2005; 6:355–367. [PubMed: 16240240]

Chong SW, Emelyanov A, Gong Z, Korzh V. Expression pattern of two zebrafish genes, cxcr4a and cxcr4b. Mech. Dev. 2001; 109:347–354. [PubMed: 11731248]

Dagia NM, Kamath DV, Bhatt P, Gupte RD, Dadarkar SS, Fonseca L, Agarwal G, Chetrapal-Kunwar A, Balachandran S, Srinivasan S, Bose J, Pari K, C BR, Parkale SS, Gadekar PK, Rodge AH, Mandrekar N, Vishwakarma RA, Sharma S. A fluorinated analog of ISO-1 blocks the recognition and biological function of MIF and is orally efficacious in a murine model of colitis. Eur. J. Pharmacol. 2009; 607:201–212. [PubMed: 19239912]

Dambly-Chaudière C, Cubedo N, Ghysen A. Control of cell migration in the development of the posterior lateral line: antagonistic interactions between the chemokine receptors CXCR4 and CXCR7/RDC1. BMC Dev. Biol. 2007; 7:23. [PubMed: 17394634]

Deverman BE, Patterson PH. Cytokines and CNS development. Neuron. 2009; 64:61–78. [PubMed: 19840550]

Esumi N, Budarf M, Ciccarelli L, Sellinger B, Kozak CA, Wistow G. Conserved gene structure and genomic linkage for D-dopachrome tautomerase (DDT) and MIF. Mamm. Genome. 1998; 9:753–757. [PubMed: 9716662]

Feng Y, Xu Q. Pivotal role of hmx2 and hmx3 in zebrafish inner ear and lateral line development. Dev. Biol. 2010; 339:507–18. [PubMed: 20043901]

Hertzano R, Puligilla C, Chan SL, Timothy C, Depireux DA, Ahmed Z, Wolf J, Eisenman DJ, Friedman TB, Riazuddin S, Kelley MW, Strome SE. CD44 is a marker for the outer pillar cells in the early postnatal mouse inner ear. J. Assoc. Res. Otolaryngol. 2010; 11:407–418. [PubMed: 20386946]

Holmes, KE.; Wyatt, MJ.; Shen, YC.; Thompson, DA.; Barald, KF. Direct Delivery of MIF Morpholinos Into the Zebrafish Otocyst by Injection and Electroporation Affects Inner Ear Development.. J. Vis. Exp. 2011. http://www.jove.com/index/Details.stp?ID=2466. doi: 10.3791/2466

Ito K, Yoshiura Y, Ototake M, Nakanishi T. Macrophage migration inhibitory factor (MIF) is essential for development of zebrafish, Danio rerio. Dev. Comp. Immunol. 2008; 32:664–672. [PubMed: 18068224]

Kobayashi S, Satomura K, Levsky JM, Sreenath T, Wistow GJ, Semba I, Shum L, Slavkin HC, Kulkarni AB. Expression pattern of macrophage migration inhibitory factor during embryogenesis. Mech. Dev. 1999; 84:153–156. [PubMed: 10473131]

Koda M, Nishio Y, Hashimoto M, Kamada T, Koshizuka S, Yoshinaga K, Onodera S, Nishihira J, Moriya H, Yamazaki M. Up-regulation of macrophage migration-inhibitory factor expression after

compression-induced spinal cord injury in rats. Acta Neuropathol. 2004; 108:31–36. [PubMed: 15067555]

Larson DF, Horak K. Macrophage migration inhibitory factor: controller of systemic inflammation. Crit Care. 2006; 10:138. [PubMed: 16677407]

Lefebvre PP, Leprince P, Weber T, Rigo JM, Delree P, Moonen G. Neuronotrophic effect of developing otic vesicle on cochleo-vestibular neurons: evidence for nerve growth factor involvement. Brain Res. 1990; 507:254–260. [PubMed: 2337765]

Leng L, Metz CN, Fang Y, Xu J, Donnelly S, Baugh J, Delohery T, Chen Y, Mitchell RA, Bucala R. MIF signal transduction initiated by binding to CD74. J. Exp. Med. 2003; 197:1467–1476. [PubMed: 12782713]

Lubetsky JB, Dios A, Han J, Aljabari B, Ruzsicska B, Mitchell R, Lolis E, Al-Abed Y. The tautomerase active site of macrophage migration inhibitory factor is a potential target for discovery of novel anti-inflammatory agents. J. Biol. Chem. 2002; 277:24976–24982. [PubMed: 11997397]

Lugrin J, Ding XC, Le Roy D, Chanson AL, Sweep FC, Calandra T, Roger T. Histone deacetylase inhibitors repress macrophage migration inhibitory factor (MIF) expression by targeting MIF gene transcription through a local chromatin deacetylation. Biochim. Biophys. Acta. 2009; 1793:1749–1758. [PubMed: 19747950]

McGrath KE, Koniski AD, Maltby KM, McGann JK, Palis J. Embryonic expression and function of the chemokine SDF-1 and its receptor, CXCR4. Dev. Biol. 1999; 213:442–456. [PubMed: 10479460]

Mitchell RA, Liao H, Chesney J, Fingerle-Rowson G, Baugh J, David J, Bucala R. Macrophage migration inhibitory factor (MIF) sustains macrophage proinflammatory function by inhibiting p53: regulatory role in the innate immune response. Proc. Natl. Acad. Sci. USA. 2002; 99:345–350. [PubMed: 11756671]

Nishino T, Bernhagen J, Shiiki H, Calandra T, Dohi K, Bucala R. Localization of macrophage migration inhibitory factor (MIF) to secretory granules within the corticotrophic and thyrotrophic cells of the pituitary gland. Mol. Med. 1995; 1:781–788. [PubMed: 8612200]

Nishio Y, Minami A, Kato H, Kaneda K, Nishihira J. Identification of macrophage migration inhibitory factor (MIF) in rat peripheral nerves: its possible involvement in nerve regeneration. Biochim. Biophys. Acta. 1999; 1453:74–82. [PubMed: 9989247]

Nishio Y, Nishihira J, Ishibashi T, Kato H, Minami A. Role of macrophage migration inhibitory factor (MIF) in peripheral nerve regeneration: anti-MIF antibody induces delay of nerve regeneration and the apoptosis of Schwann cells. Mol. Med. 2002; 8:509–520. [PubMed: 12456989]

Noh EJ, Lim DS, Jeong G, Lee JS. An HDAC inhibitor, trichostatin A, induces a delay at G2/M transition, slippage of spindle checkpoint, and cell death in a transcription-dependent manner. Biochem. Biophys. Res. Commun. 2009; 378:326–31. [PubMed: 19038231]

Purves, D.; Augustine, GJ.; Fitzpatrick, D.; Katz, LC.; LaMantia, A-S.; James, O.; McNamara, JO.; S Mark Williams, SM. Neuroscience. 2nd edition. Sinauer Associates; Sunderland (MA): 2001.

Shen YC, Jeyabalan AK, Wu KL, Hunker KL, Kohrman DC, Thompson DL, Liu D, Barald KF. The transmembrane inner ear (tmie) gene contributes to vestibular and lateral line development and function in the zebrafish (Danio rerio). Dev. Dyn. 2008; 237:941–952. [PubMed: 18330929]

Shen YC, Raymond PA. Zebrafish cone-rod (crx) homeobox gene promotes retinogenesis. Dev. Biol. 2004; 269:237–251. [PubMed: 15081370]

Suzuki M, Takamura Y, Maeno M, Tochinai S, Iyaguchi D, Tanaka I, Nishihira J, Ishibashi T. *Xenopus* laevis macrophage migration inhibitory factor is essential for axis formation and neural development. J. Biol. Chem. 2004; 279:21406–21414. [PubMed: 15024012]

Takahashi A, Iwabuchi K, Suzuki M, Ogasawara K, Nishihira J, Onoe K. Antisense macrophage migration inhibitory factor (MIF) prevents anti-IgM mediated growth arrest and apoptosis of a murine B cell line by regulating cell cycle progression. Microbiol. Immunol. 1999; 43:61–67. [PubMed: 10100748]

Tissir F, Wang CE, Goffinet AM. Expression of the chemokine receptor Cxcr4 mRNA during mouse brain development. Brain Res Dev Brain Res. 2004; 149:63–71.

Tiveron MC, Cremer H. CXCL12/CXCR4 signalling in neuronal cell migration. Curr. Opin. Neurobiol. 2008; 18:237–244. [PubMed: 18644448]

Valentin G, Haas P, Gilmour D. The chemokine SDF1a coordinates tissue migration through the spatially restricted activation of Cxcr7 and Cxcr4b. Curr. Biol. 2007; 17:1026–1031. [PubMed: 17570670]

Waterman RE, Bell DH. Epithelial fusion during early semicircular canal formation in the embryonic zebrafish, Brachydanio rerio. Anat. Rec. 1984; 210:101–114. [PubMed: 6486477]

Weiser WY, Temple PA, Witek-Giannotti JS, Remold HG, Clark SC, David JR. Molecular cloning of a cDNA encoding a human macrophage migration inhibitory factor. Proc. Natl. Acad. Sci. USA. 1989; 86:7522–7526. [PubMed: 2552447]

Westerfield, M. A guide for the laboratory use fo zebrafish (Danio rerio). University of Oregen Press; Eugene, OR: 2000. The Zebrafish Book..

Wilson AL, Shen YC, Babb-Clendenon SG, Rostedt J, Liu B, Barald KF, Marrs JA, Liu Q. Cadherin-4 plays a role in the development of zebrafish cranial ganglia and lateral line system. Dev. Dyn. 2007; 236:893–902. [PubMed: 17279575]

Winner M, Meier J, Zierow S, Rendon BE, Crichlow GV, Riggs R, Bucala R, Leng L, Smith N, Lolis E, Trent JO, Mitchell RA. A novel, macrophage migration inhibitory factor suicide substrate inhibits motility and growth of lung cancer cells. Cancer. Res. 2008; 68:7253–7257. [PubMed: 18794110]

Yoder JA, Haire RN, Litman GW. Cloning of two zebrafish cDNAs that share domains with the MHC class II-associated invariant chain. Immunogenetics. 1999; 50:84–88. [PubMed: 10541812]

Yoshimoto T, Nishihira J, Tada M, Houkin K, Abe H. Induction of macrophage migration inhibitory factor messenger ribonucleic acid in rat forebrain by reperfusion. Neurosurgery. 1997; 41:648–653. [PubMed: 9310983]

Zou YR, Kottmann AH, Kuroda M, Taniuchi I, Littman DR. Function of the chemokine receptor CXCR4 in haematopoiesis and in cerebellar development. Nature. 1998; 393:595–599. [PubMed: 9634238]

Highlights

>Cytokines and sensory systems: MIF plays a critical role in shaping inner ear innervation

>Immune system cytokines generated by the developing otocyst influence directional outgrowth and survival of inner ear neurons

>Receptors for the neurotrophic cytokine MIF resembling those of the immune system are expressed on embryonic and adult inner ear neurons

>Blocking either MIF or MIF receptors with antisense oligonucleotide morpholinos has profound effects on inner ear development

>MIF effects are mediated at least partially through p53 pathways

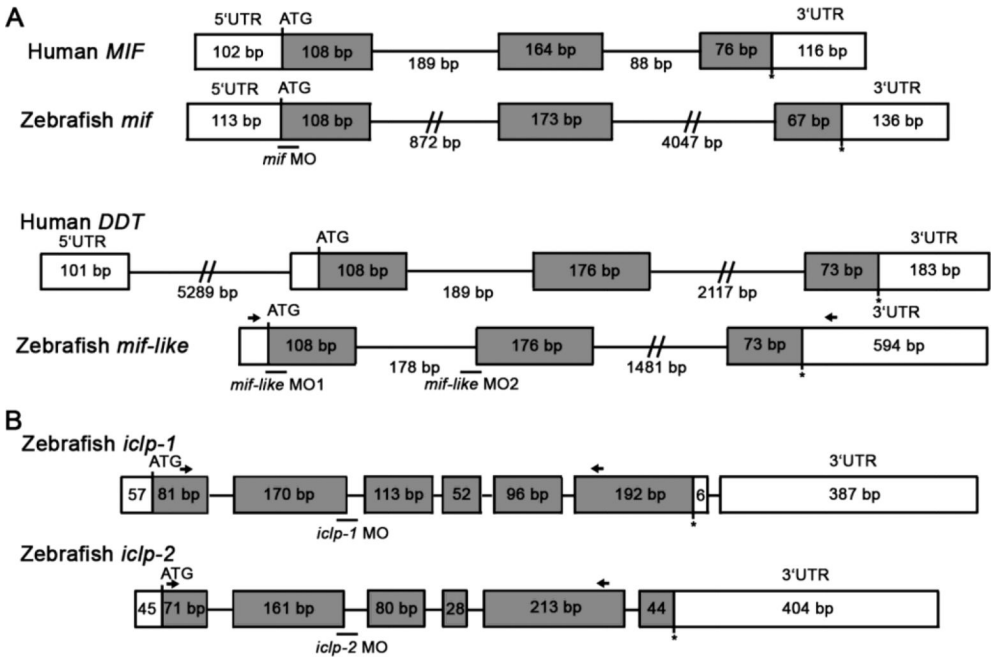

Fig. 1. Gene structures of zebrafish *mif, mif-like, iclp1*, and *iclp2*

(A) Comparison of zebrafish *mif*, *mif-like* and their human orthologs. Gray boxes: open reading frames for the predicted proteins; white boxes: untranslated regions; lines indicate introns; Stars: stop codons. Positions of morpholinos (MOs) are underlined. Arrows indicate the primers used to obtain RT-PCR products in Figs. 2 and 4. (B) Genomic structure of zebrafish *iclp1* and *iclp2*. MO positions indicated. Arrows indicate primers for RT-PCR products in Figs. 3 and 4.

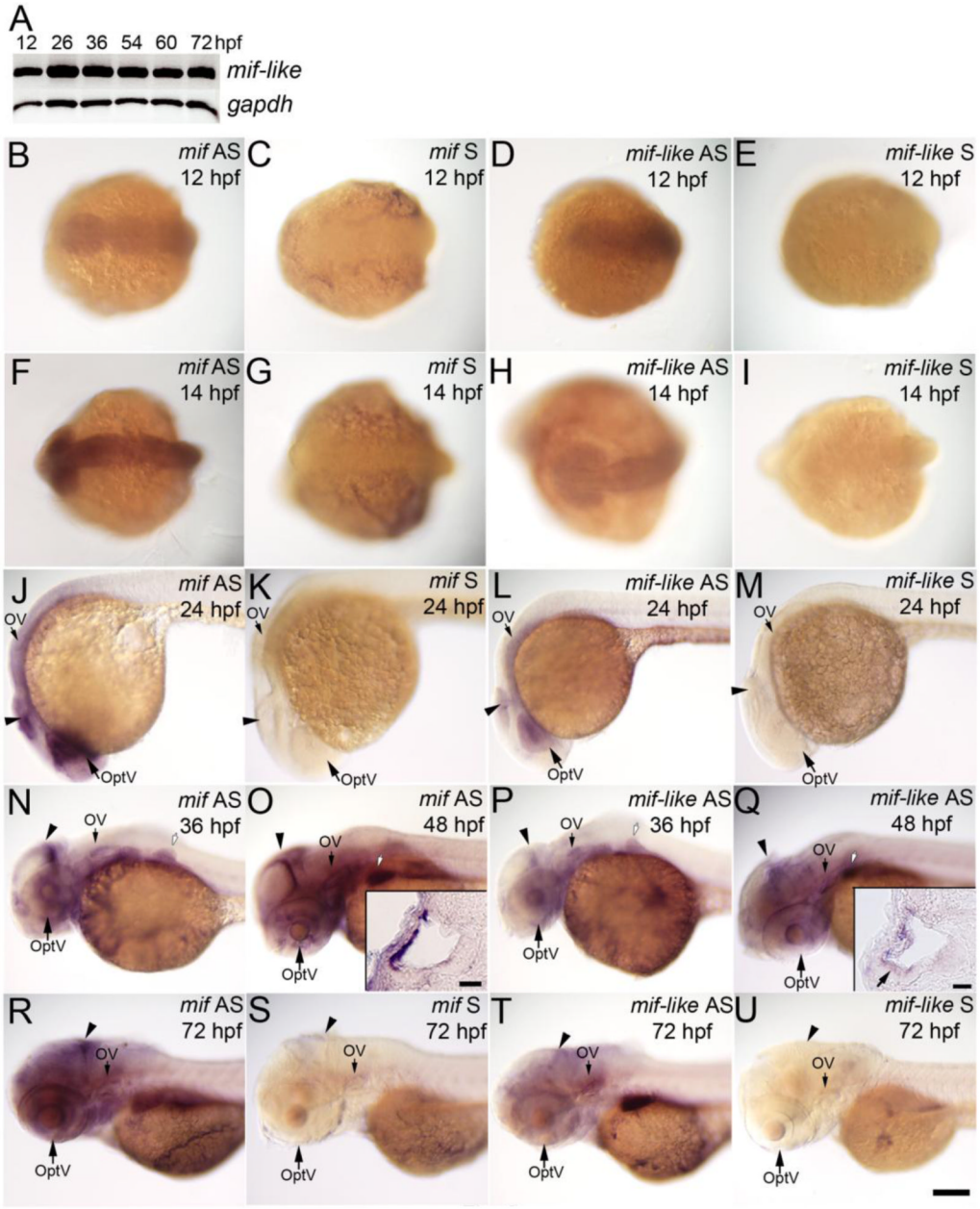

Fig. 2. Expression of *mif* and *mif-like* transcripts in the brain, eye and ear during embryogenesis

(A) RT-PCR results of *mif-like* mRNA from whole embryos at 12, 26, 36, 54, 60, and 72 hpf. (B-U) Whole mount ISH with *mif* or *mif-like* probes. (B-E) Dorsal view of 12-hpf embryos; (F-I) Dorsal view of 14-hpf embryos; (J-M) Lateral view of 24-hpf embryos; (N, P) Lateral view of 36-hpf embryos; (O, Q) Lateral view of 48-hpf embryos; (R-U) Lateral view of 72-hpf larvae. (B, F, J, N, O, R) *mif* antisense probe; (C, G, K, S) *mif* sense probe; (D, H, L, P, Q, T) *mif-like* anti-sense probe; (E, I, M, U) *mif-like* sense probe. Insets in (O) and (Q) show transverse sections through the ear; the small arrow in inset (Q) indicates hair cells in the anterior macula. Arrowheads: brain; OptV: optic vesicle; OV: otic vesicle; white arrows with black outlines: pectoral fin bud. Scale bar: 100 μm for (B-U); 20 μm for insets.

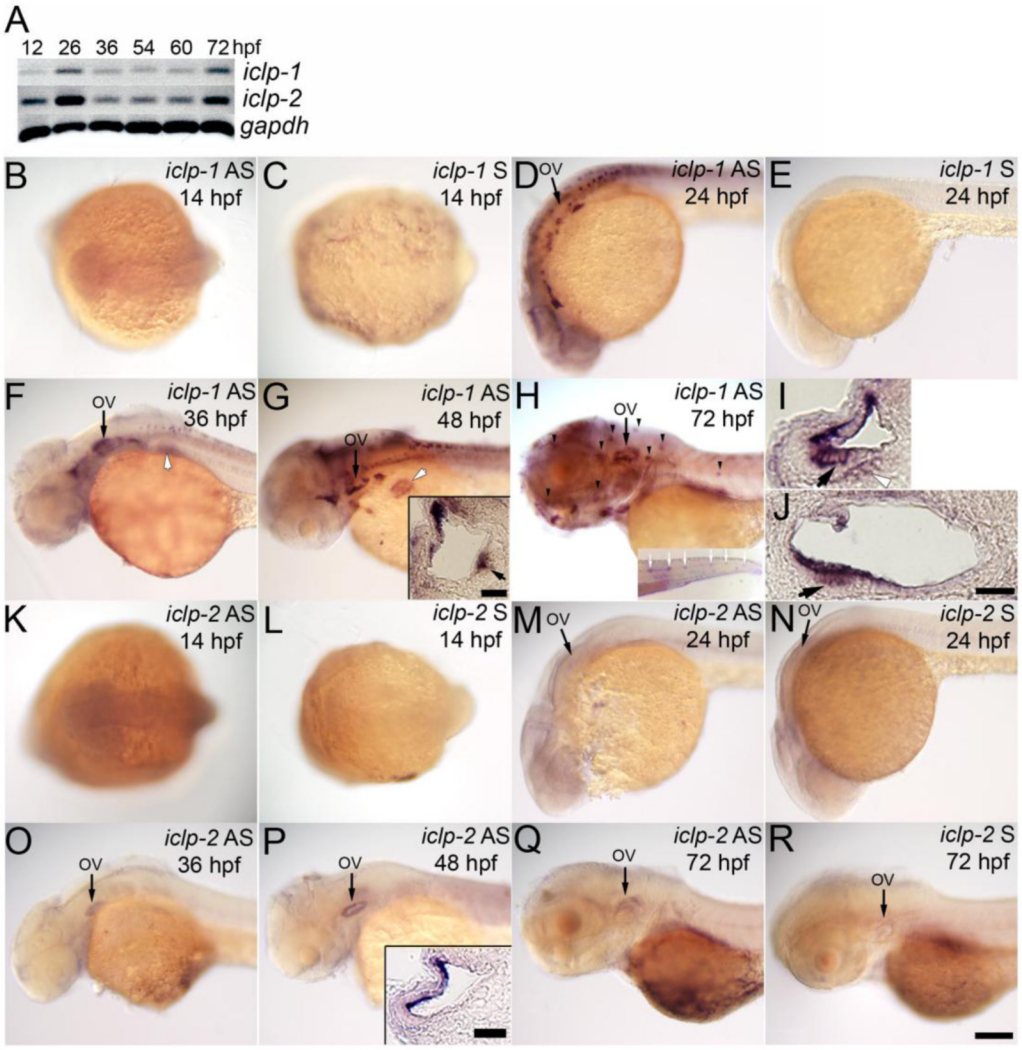

Fig. 3. Expression patterns of embryonic *iclp1* and *iclp2*

(A) RT-PCR results of *iclp1* and *iclp -2* transcripts from whole embryos of 12, 26, 36, 54, 60, and 72 hpf. (B-H, K-R) Whole mount ISH with *iclp1* (B-H) *or iclp2* (K-R) probes. (B, C, K, L) Dorsal view of 14-hpf embryos; (D-H, M-R) Lateral view of (D, E, M, N) 24-hpf embryos; (F, O) 36-hpf embryos; (G, P) 48-hpf embryos; (H, Q, R) 72-hpf larvae. (B, D, F, G, H) with *iclp1* antisense probe; (C, E) with *iclp1* sense probe; (K, M, O, P, Q) with *iclp2* antisense probe; (L, N, R) with *iclp2* sense probe. (I, J) *iclp1* labeling of 48 hpf embryo with transverse (I) and sagittal (J) sections. Arrows in (I) and (J) indicate hair cells in the anterior macula. Insets in (G) and (P) show transverse sections of the ear; Inset (G) inset shows a section through the posterior macula; small arrow in inset (G) indicates hair cells in the sensory patches. Inset (H) shows a tail with posterior LL neuromast staining. OV: otic vesicle. Arrowheads: anterior LL neuromasts; white arrows: posterior LL neuromasts; white arrows with black outlines: pectoral fin bud; white arrowhead with black outline: statoacoustic ganglion (SAG). Scale bar: 100 μm for (B-H) and (K-R); 20 μm for insets, (I) and (J).

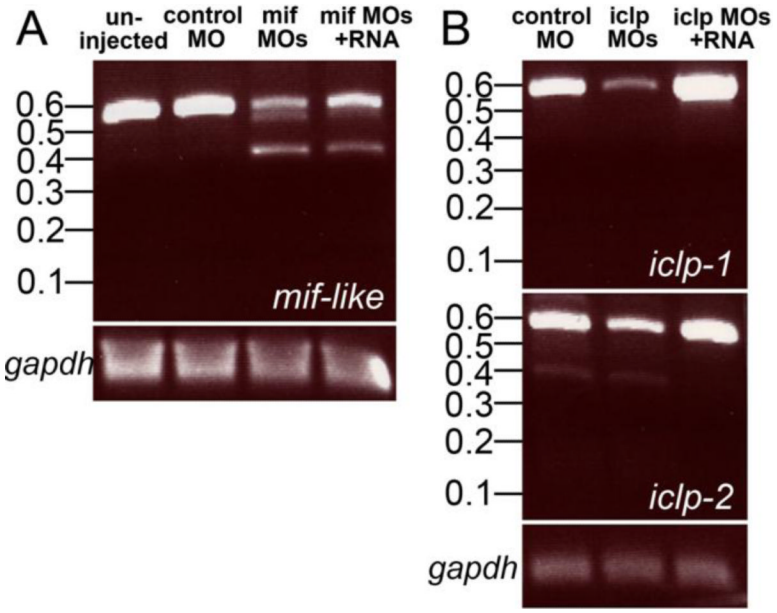

Fig. 4. Morpholinos reduced the levels of normal transcripts of *mif-like, iclp1,* and *iclp2*

(A) RT-PCR of *mif-like* transcripts from uninjected, control MO injected, *mif* morpholinos injected and mif morpholinos plus capped RNAs injected 50-hpf embryos. Predicted size of normal transcript is 512 bp; predicted transcript blocked by *mif-like* MO = 336 bp. (B) RT-PCR of *iclp1* and *iclp2* transcripts from control MO-injected, *iclp* morpholinos injected and *iclp* morpholinos plus capped RNAs injected 50-hpf embryos. Predicted size of normal *iclp1* product =523 bp, transcript lacking exon 2 = 353 bp. Predicted size of normal *iclp2* product = 525 bp, transcript lacking exon 2 = 364 bp.

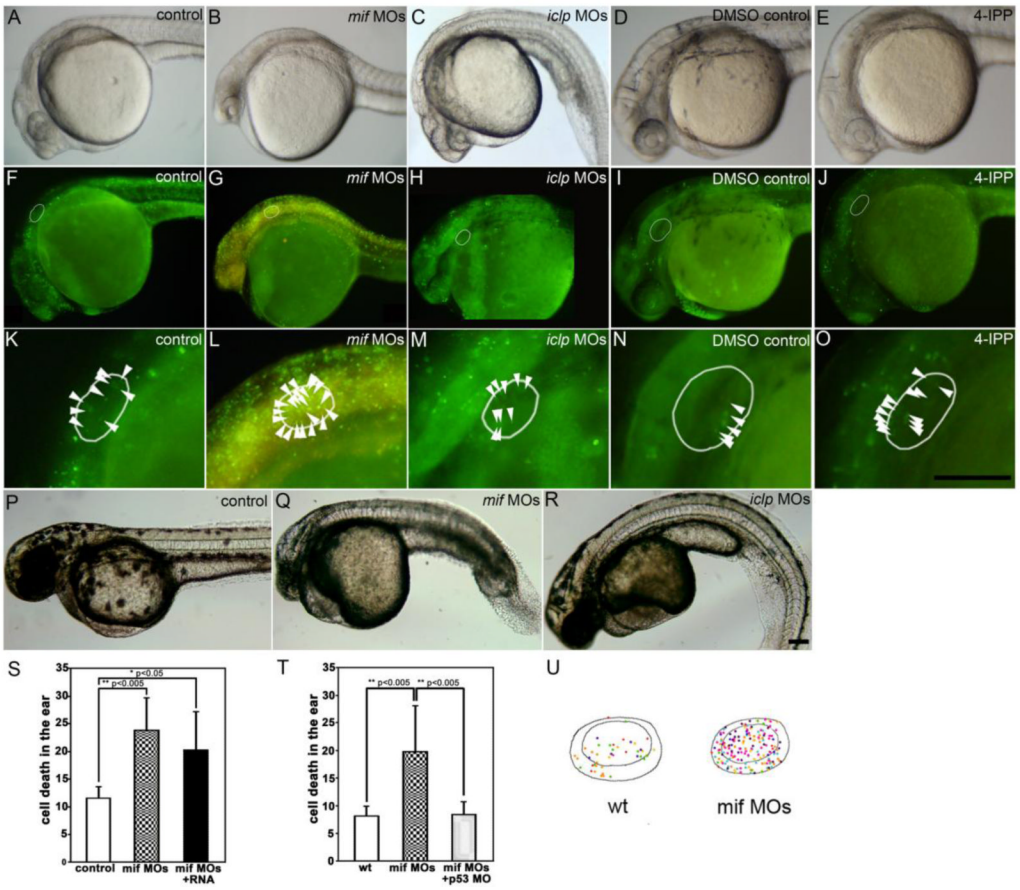

Fig. 5. Gross morphology was affected by *mif* and *iclp* morpholinos

Lateral view of embryos at 29 hpf (A-E) and 48 hpf (P-R). (F-O) Acridine orange (AO) staining demonstrated cell death in 29-hpf embryos. (K-O) Magnified ear area in (F-J) respectively. (A, F, K, P) control; (B, G, L, Q) *mif* morphants; (C, H, M, R) *iclp* morphants; (D, I, N) DMSO control; (E, J, O) 4-IPP (40 μM)-treated embryos. White oval outlines indicate the positions of the otocysts; white arrowheads point to the AO-stained cells in the otocysts. (S, T) Comparison of AO-stained cells in the inner ear (n=4 for each treatment in (S), and n=5 for wt, 8 for both *mif* MOs and *mif* MOs+p53 MO in (T)) at 29 hpf. (U) Illustration of the location of AO-positive cells in the otocyst. The different colors of the spots represent AO-positive cells in the different embryos assessed. They are superimposed in this figure to determine if cells in a particular region were more susceptible (n=5 for wild type, and 8 for *mif* morphants). Scale bar: 100 μm.

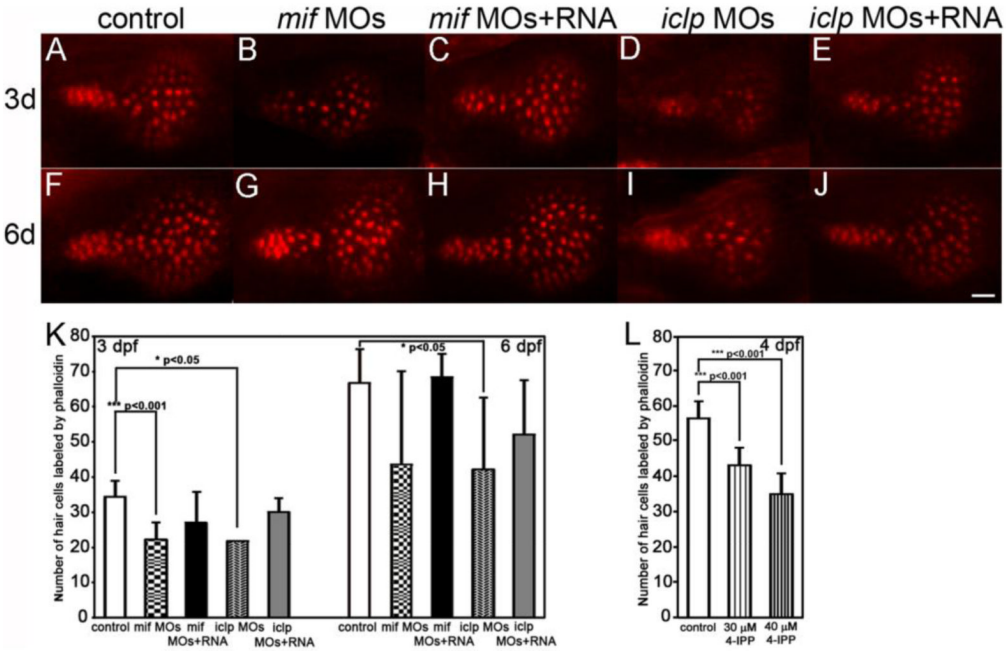

Fig. 6. Phalloidin staining of the sensory hair patch showed defects in *mif* and *iclp* morphants

(A-J) Phalloidin staining of saccular macula with 3d (A-E) and 6d (F-J) larvae. Anterior is to the left. (K) Numbers of HC labeled by phalloidin at 3dpf (n= 9 for control, 10 for *mif* morphants, 13 for *mif* morphants with RNA rescue, 2 for *iclp* morphants, 6 for *iclp* morphants with capped RNA) and 6 dpf (n=4 for control, 7 for *mif* morphants, 3 for *mif* morphants with RNA rescue, 5 for *iclp* morphants, 6 for *iclp* morphants with capped RNA). (L) Numbers of HC labeled by phalloidin at 4 hpf (n=14 for DMSO control, 9 for 30 μM 4-IPP, 12 for 40 μM 4-IPP treatment). Scale bar: 10 μm.

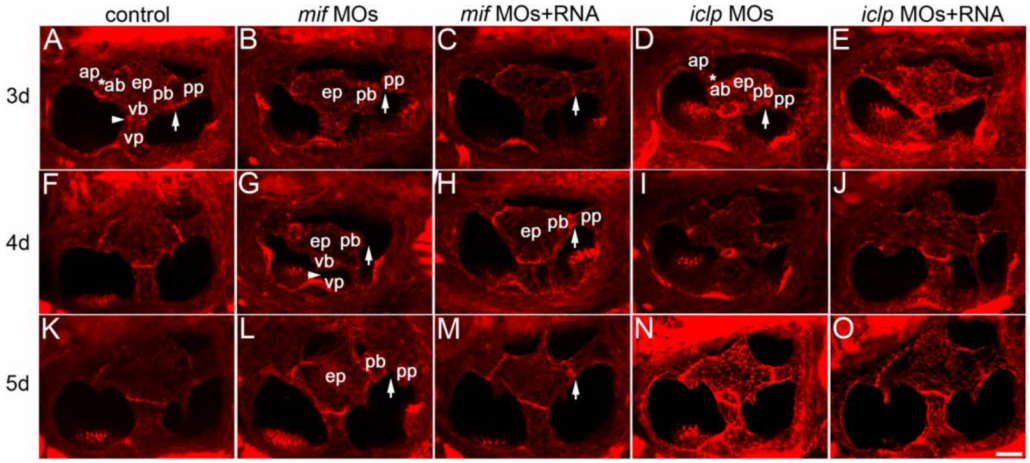

Fig. 7. Semicircular canal formation in *mif* and *iclp* morphants

(A-O) phalloidin staining of epithelial pillars (ep), which form hubs of the developing SCC. (A-E) 3dpf; (F-J) 4dpf; (K-O) 5dpf larvae. (A, F, K) control; (B, G, L) *mif* morphants; (C, H, M) *mif* morphants with capped *mif* RNAs; (D, I, N) *iclp* morphants; (E, J, O) *iclp* morphants with capped *iclp* RNAs. Anterior is to the left. Arrows: junction of the posterior bulge (pb) and posterior protrusion (pp). Arrowheads: junction between the ventral bulge (vb) and ventral protrusion (vp). Stars: junction of the anterior protrusion (ap) and the anterior bulge (ab). In *mif* morphants, a gap between the pb and the pp was observed, indicating fusion failure. Scale bar: 25 μm. n=11 for the 3 dpf control, 12 for the 3dpf mif morphants, 4 for the 3dpf mif MOs+RNA. Among the 12 mif morphants, 9 had defects in SCC formation (75%). n for 4 dpf is 7 for the controls, 6 for the mif morphants, 6 for the mif MOs+RNA, 11 for the iclp morphants, 5 for the iclp MOs+RNA. Four out of 6 (67%) mif morphants had SCC defects. For 5 dpf larvae, n=6 for control, 7 for mif morphants, 7 for mif MOs+RNA, 5 for iclp morphants, 6 for iclp MOs+RNA. Eighty six percent (6 out of 7) mif morphants had SCC defects.

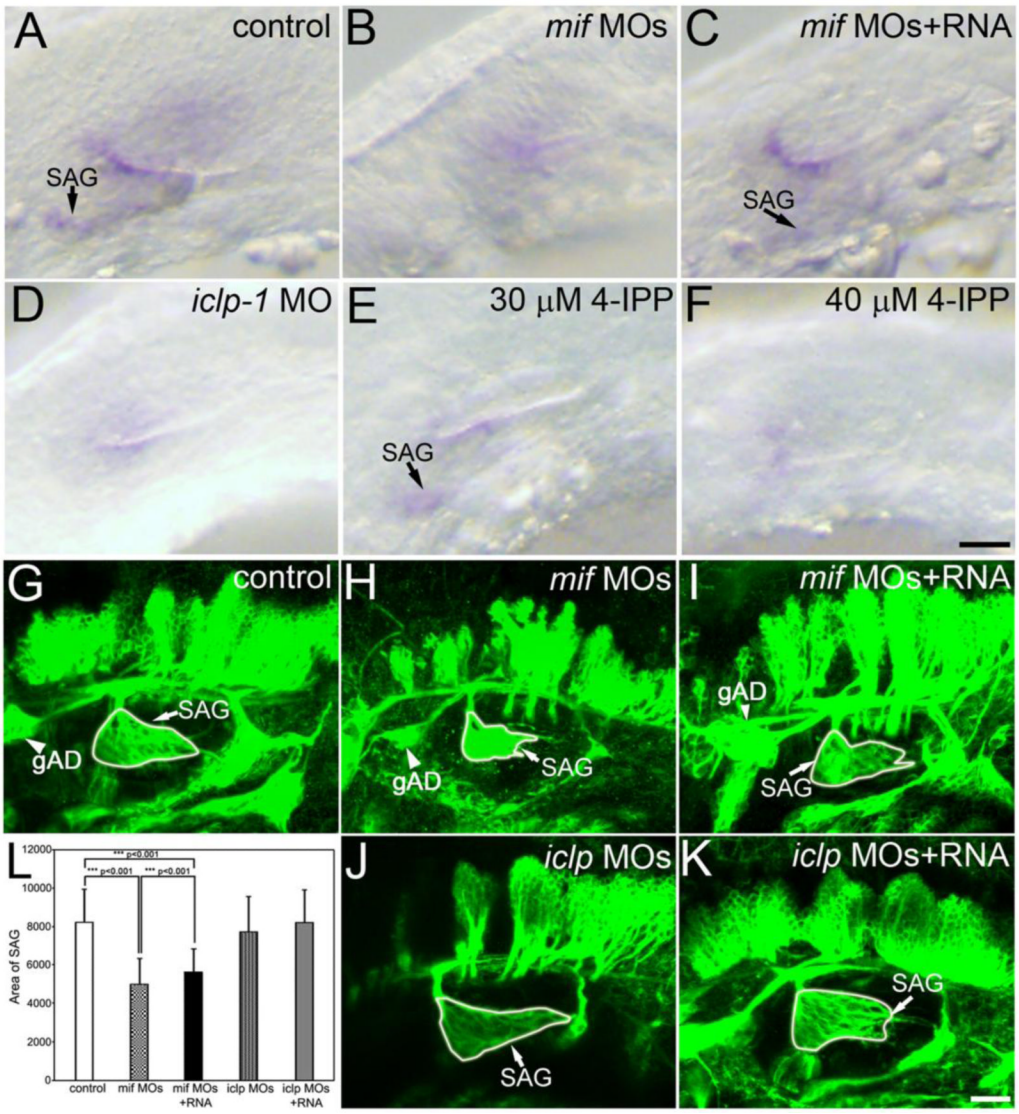

Fig. 8. Statoacoustic ganglion in the *mif, iclp* morphants and 4-IPP treated embryos

(A-F) Whole mount in situ hybridization of embryos with an *nkx5.1* probe, showing the otic vesicle and SAG at 32 hpf. (A) control embryo; (B) *mif* morphant; (C) *mif* morphant with RNA; (D) *iclp1* morphant; (E, F) 4-IPP treated (E: 30 μM, F: 40 μM) embryos. (G-K) zn-5 staining in 48-hpf embryos. (G) control; (H) *mif* morphant; (I) *mif* morphant with capped *mif* RNAs; (J) *iclp* morphant; (K) *iclp* morphant with capped *iclp* RNAs. The white line outlines the SAGs. Note other cranial ganglia were also smaller in the *mif* morphants than the control. gAD: anterodorsal LL ganglia. Scale bar: 25 μm. (L) Comparison of size of the SAG with various treatments. Control embryos (n=30), *mif* MOs (n=14), *mif* MOs+RNA (n=12), *iclp* MOs (n=17), and *iclp* MOs+RNA (n=15).

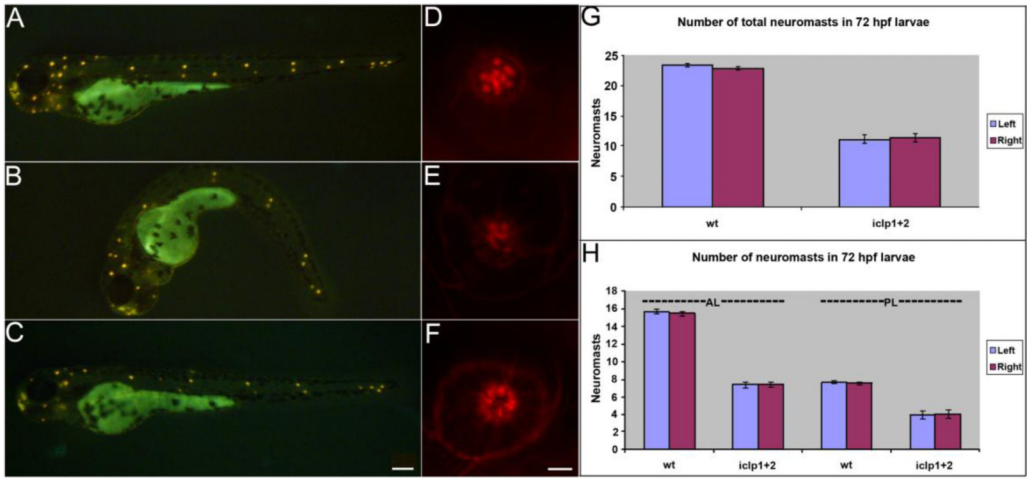

Fig. 9. Development of lateral line (LL) in iclp morphants

(A-C) 4-Di-2-ASP staining of 72-hpf control (A), *iclp* morphant (B), and *iclp* morphant with capped RNAs (C). (D-F) Phalloidin staining of posterior LL neuromast at 5 dpf in control (D), *iclp* MOs-injected (E), and *iclp* MOs plus RNA-injected (F) larvae. Scale bar: 100 μm for (A-C), 5 μm for (D-E). (G, H) Comparison of numbers of neuromast stained with 4-Di-2-ASP in control larvae and *iclp* morphants. Wt (n=10), MO (n=15).